Materials and Corrosion / Werkstoffe und Korrosion, Volume 68, Issue 2, February 2017, pp. 205–214
DOI:10.1002/maco.201508779

Article type: Article

Title: Modelling Gas Turbine Materials' Hot Corrosion Degradation in Combustion Environments from H_2-rich Syngas

Joy Sumner, Andrew Potter, Nigel J. Simms, John E. Oakey

Joy Sumner
Cranfield University, Cranfield, Bedfordshire, MK43 0AL, UK
j.sumner@cranfield.ac.uk

Andrew Potter
Cranfield University, Cranfield, Bedfordshire, MK43 0AL, UK

Nigel J. Simms
Cranfield University, Cranfield, Bedfordshire, MK43 0AL, UK

John E. Oakey
Cranfield University, Cranfield, Bedfordshire, MK43 0AL, UK

Components of gas turbines (such as blades, vanes, combustor cans) exposed to combustion environments at high temperature are susceptible to hot corrosion attack. To successfully plan maintenance and to determine whether to operate in novel combustion modes (for example, in integrated gasification combined cycles that incorporate pre-combustion carbon capture) predictions of hot corrosion component life must be made.

In this paper, hot corrosion datasets relating to 2 alloys, MarM 509 (a cobalt-based superalloy) and Rene 80 (a nickel-based superalloy) form the basis of hot corrosion predictive lifetime models. The model framework is based on the two stages of incubation and propagation, with the transitions from incubation to propagation around the samples being based on Weibull statistics.

The impact of a range of temperatures (including 700 °C and 900 °C), gas compositions (simulating the combustion of natural gas, H_2-rich syngas, or partially cleaned syngas) and deposit chemistries/fluxes have been assessed. Predictions have been made including the expected damage spread for a range of different exposure conditions.

Keywords: modelling; incubation; propagation; Weibull statistics; H_2-IGCC; hot corrosion; lifetime; Rene 80; MarM 509; superalloys

1. Introduction

To meet European Union CO_2 emission reduction targets (e.g. for 2020, 2030 and 2050 [1,2]), technologies capable of enabling carbon capture and storage (CCS) are being increasingly investigated. One of these technologies involves the use of pre-combustion CO_2 capture and storage (CCS) incorporated into an integrated gasification combined cycle (IGCC) to reduce net CO_2 emissions [3-5].

In this instance, following the gasification of a solid fuel such as coal, a syngas (or fuel gas) containing CO-CO_2-H_2-H_2O-H_2S-etc is produced. This syngas is then cooled to go through additional cleaning stages before its combustion in an industrial gas turbine (IGT). These stages incorporate improved H_2S/COS-removal [6] (to protect later catalysts), as well as the removal of particulate matter. Water-gas shift reactors are used to alter the syngas composition, lowering the levels of CO and H_2O and raising the concentrations of H_2 and CO_2.

Due to the high levels of CO_2 present, the majority of this can then be removed [3,4,7] before the resulting H_2-rich syngas is then combusted in the IGT.

Combusting the H_2-rich syngas within the IGT will lead to proportionally higher levels of H_2O in the combusted gas stream than are found when combusting either conventional syngas or natural gas. This has the potential to affect components (such as the blades, vanes and combustor cans) in this hot combusted gas stream [8,9].

In addition to operating using H_2-rich syngas, other potential fuel gas compositions need to be investigated. In the event that one of the gas clean-up stages fails, it is necessary to bypass the water-gas shift reactor to ensure that the catalyst is not poisoned [6]. As such, the resulting partially cleaned syngas would produce a combusted gas environment with a lower H_2O content but higher SO_X content than the H_2-rich syngas. (It should be noted that the H_2O levels in this event will be lower than for combustion of natural gas, assuming that bitumous coal has been gasified.)

Hot corrosion is a complex phenomenon and the presence of SO_X is known to enhance the rate of attack [10], especially for type II hot corrosion (characteristically peaking at 700 °C and resulting in pitting damage). At the lower temperatures of type II hot corrosion, the SO_X contains a greater fraction of SO_3 which stabilises the formation of base metal sulphates. These base metal sulphates can then form low melting point mixtures with deposits (alkali metal sulphates, chlorides, etc) that would otherwise be solid over that temperature regime [11].

An EU Framework 7 project, "H2-IGCC", was established to look at the viability of IGCC power generation cycles with the incorporation of pre-combustion carbon capture, including: the performance of gas turbine materials; combustion of H_2-rich syngases for gas turbines; and modified turbo-machinery designs to enable the use of H_2-rich syngases. The degree to which these novel combusted gas environments are anticipated to affect materials exposed in the hot, combusted gas stream has been established by exposing over 600 samples in hot corrosion exposures, as reported elsewhere [12,13]. These tests investigated the effect of the 3 previously described combustion environments on a range of state-of-the-art alloys and coating systems for different temperatures and deposit compositions/fluxes.

The development of predictive modelling of the potential lifetimes of candidate materials' was one of the project outputs and is important for life predictions in the field. Thus such a model is reported in this paper for two example materials systems, Rene 80 and MarM 509. The implication that these model outputs have for the potential operation of H_2-rich syngas-fired IGCC plant is also discussed.

2. Methodology

The following three sub-sections cover: (a) how the hot corrosion tests were run to gather data to build the model; (b) the analysis method used to obtain quantifiable data on corrosion damage levels; and, (c) the steps for building the model.

2.1 Acquisition of Experimental Data

Samples were produced from a range of state-of-the-art materials systems used in IGTs. In addition to coated samples, uncoated samples were also produced as not all parts of hot gas

path components are coated and the degree of coating and proportion of coated stages vary between IGT manufacturers (though there are generally more uncoated stages in older IGT designs). Furthermore, in instances where coatings have spalled, corroded or otherwise been damaged, it is important to understand the remaining life of the component. In particular, this paper addresses the hot corrosion metal loss for samples of uncoated Rene 80 and MarM 509 (compositions in Table 1). The raw superalloy was machined into linked spools of cylindrical samples (each ~10 mm long and ~10 mm in diameter). Later the links between the spools were severed to produce individual samples for testing, which were exposed with as-machined surfaces (R_a < 0.4 μm).

A range of hot corrosion testing methodologies exist [14-17]. Hot corrosion testing was conducted using the "deposit recoat" method [18], which is in line with one of the standard test methodologies (e.g. [14]), to simulate the three anticipated combustion environments. For the experiments, a controlled atmosphere furnace raised the samples to a suitable temperature (here either 700 °C or 900 °C to simulate type II and type I hot corrosion respectively) while a corrosive gas of suitable composition flowed around samples coated in a corrosive deposit. The corrosive deposit was re-applied every 100 hours and weight change data collected. Samples were removed for destructive analysis by cross-sectioning after 100, 300 or 500 hours.

Table 2 gives the three different compositions of the gas flowing in the vertical, controlled atmosphere furnaces, while Table 3 gives deposit compositions and fluxes. Gas compositions were selected following assessments of the expected fuel gases, air:fuel ratios, and gas cleaning steps of likely advanced IGCC cycles. As the hot corrosion testing furnaces operated at lower pressures than the IGTs (1 bar compared to ~15 bar), the partial pressures of the SO_X

were kept constant [12]. Dry gases were purchased from BOC and the required steam content added using a peristaltic pump. To prevent reactions between the gas and furnace (including furnace furniture), surfaces in contact with the gas were produced from alumina.

The temperatures selected for discussion in this paper were 700 and 900 °C. Part of the reason for the selection of these temperatures was the different damage mechanisms that they typically produce [10,11]. At 700 °C, type II hot corrosion is expected; this is often characterised by pitting. At 900 °C, type I hot corrosion is expected; this is often characterised by internal damage in the form of sulphides ahead of broad fronted oxidation/sulphidation attack. As the internal sulphides are typically weak, regions of a component were these are present within the metal matrix, are no longer sound. It should be noted that, unlike cooled components operating in a gas turbine, samples in the furnace are subjected to a constant temperature through their cross-section.

2.2 Image Analysis Technique

Weight change measurements were taken every 100 hours, to help assess the degree of corrosion. However, as pitting and internal damage will not result in large weight changes, and as spallation is a common problem with corroded samples, dimensional metrology data were also collected. For the dimensional metrology data, pre-exposure measurements of the sample were compared to post-exposure image analyser/optical microscopy measurements to determine both the degree of metal loss (ML) and of good metal loss (GML = metal loss + internal damage). The extents of ML and GML were plotted as a function of cumulative probability (assuming a normal distribution) in standard deviations from the median (std. dev.) [19-22]. This analysis produced statistically significant datasets (with an error of ±5 µm) which allowed comparison between different systems and environments. The

dimensional metrology technique is described in more detail in references [23-25]. The application of these statistics to hot corrosion metal losses are also illustrated in ISO standards [22,26,27]. More recently, this statistical approach to corrosion degradation has been used in a range of environments, e.g., [28,29].

Post-exposure, samples were imaged by a scanning electron microscope (SEM) equipped with energy dispersive X-ray spectroscopy (EDX) to study the microstructural evolution.

2.3 Model Construction

Hot corrosion damage proceeds via two distinct sequential stages. Initially a protective layer exists on the sample and, for some time (incubation period), this keeps GML rates low. At some point (the incubation lifetime) however, this protective layer becomes damaged and more rapid attack of the base alloy occurs. This more rapid attack is known as the propagation stage. As such, the GML can be modelled [23]. Equation (1a) is used for times shorter than the incubation time, and Equation (1b) for times longer than the incubation time.

$$GML = k_{inc} t^n \quad (1a)$$

$$GML = k_{inc} {t_{inc}}^n + k_{prop}(t - t_{inc})^m \quad (1b)$$

Where: t is time (in hours); GML, amount of GML (in µm); n & m, powers; k_{inc}, GML rate in incubation; k_{prop}, GML rate in propagation; and t_{inc}, the incubation's duration/lifetime where the sample has been exposed for sufficient time to reach propagation (in hours).

As such, to model the progression of hot corrosion damage under a given set of conditions, these parameters must be evaluated. Determining the incubation lifetime is particularly

important. Weibull statistics have been applied to understand the spread in incubation lifetimes across a given sample (or for several samples exposed in an identical manner) [23].

3. Results and Discussion

3.1 Examples of Dimensional Metrology Data

Figure 1 shows examples of GML cumulative probability graphs for MarM 509 and Rene 80. In Figure 1(a) the evolution of hot corrosion damage with time can be followed for a series of MarM 509 samples which have been exposed to the simulated combusted partially cleaned syngas/deposit 3 at 700 °C. After 100 hours the majority of measured areas around the sample have lost less than ~10 μm. The lack of deeper localised damage indicates that these areas may be considered to be in incubation. However, at a few locations (approximately 3), more metal has been lost, indicating the initiation of hot corrosion propagation, via pitting, in these specific areas. After 300 hours more extensive GML has occurred, with the majority of the sample showing significant metal loss and undergoing hot corrosion propagation. A fraction of the surface shows pitting/more rapid metal loss. This continues at 500 hours.

The presence of these hot corrosion pits can be seen in SEM micrographs in Figure 2(a). These pits contain mixed oxides and sulphur-rich species; typical of type II hot corrosion mechanisms.

A comparison of the MarM 509 data to similar data in Figure 1(b) for Rene 80 shows that hot corrosion is progressing more rapidly in MarM 509 than Rene 80. Figure 1(c) and 1(d) show

the impact that reducing the deposit flux has on the extent of hot corrosion for these two superalloys. Additionally, where no deposit was applied, the material remains in incubation.

3.2 Modelling MarM 509 GML for Different Fluxes in Simulated Combusted Partially Cleaned Syngas

Of the corrosive environments tested, the gas simulating combusted partially cleaned syngas at 700 °C gave the most extensive GML for the tested alloys, including MarM 509 and Rene 80. As such, the model was first fitted to this, more corrosive, data. The effect of gas atmosphere will be returned to in later sections.

Using the example of MarM 509, values of k_{inc}, and k_{prop}, can be extracted from datasets showing GML advancing with time. This has been described in detail elsewhere for other materials systems [23]. Briefly, the propagation rate can be obtained by observing the change in GML with time for regions of the sample undergoing the propagation of hot corrosion, while, in an analogous manner, the incubation rate can be obtained from regions which remain in incubation.

As can be observed in Figure 1, there is a spread in degree of damage around any given sample exposed under a specific set of hot corrosion conditions. This may be considered an effect of a spread in incubation lifetimes occurring in different areas of the sample surfaces. In this instance, a range of different incubation-to-propagation transition times will result in a spread in GML values for a sample removed after a given exposure time.

Weibull distributions (Equation 2), often used in survival analysis and reliability engineering, can be used to determine this spread in incubation lifetimes by fitting two parameters: the characteristic lifetime (η) and the Weibull modulus (β) [19,23].

$$F(t) = 1 - e^{-(\frac{t}{\eta})^{\beta}} \quad (2)$$

Where, F(t) is the probability of failure at time, t. In this instance, the "failure times" used to fit the Weibull distribution correspond to the incubation lifetime for progressively larger cumulative probabilities [23].

Both the Weibull modulus and characteristic lifetime depend on the data used to fit the distribution as shown in Figure 3. Here, dimensional metrology data for the GML measurements have been taken from 30 different locations for each time period. This gives a maximum of 30 datasets from which to calculate the incubation lifetime for different cumulative probabilities. However, datasets where the sample has not moved out of incubation, or where errors are suspected, are not used to ensure that the Weibull modulus and characteristic lifetime will correctly generate the spread in incubation lifetime.

In Figure 4 the families of lines have been plotted according to Equation 1(a and b). Instead of having one line for a given set of exposure conditions with a single value of t_{inc} a series of lines representing a spread of different incubation lifetimes are plotted. These varying t_{inc} values arise from the Weibull distribution, given in Equation 2. As such, in Figure 4, the grey-scale increases from light shades at a 1% probability of the sample having moved into propagation (i.e. most of the sample will continue along the incubation GML line) to black for a 50% probability of the sample having moved into propagation (half of the sample will be

propagating, while half remains in incubation). The grey-scale then lightens again as the probability of the sample having moved into propagation rises to 99% (only a small fraction of the sample can be considered to remain in incubation, with damage predicted by the incubation line of the plot). As such, the model's outputs give the spread of GML for a given exposure time, accounting for the range in incubation lives around the sample).

Specifically, Figure 4 gives example outputs of this Weibull-based model for MarM 509 exposed at 700 °C to simulated, combusted partially cleaned syngas with different fluxes of 4/1 sodium/potassium sulphate. Data here have been plotted against cumulative normal probability in standard deviations, rather than as percentage. These have been calculated using Excel functions for standard normal cumulative probability. Plotting against normal cumulative probability (linear in standard deviations) rather than cumulative probability (linear in percentage) has the advantage of showing any underlying normal distribution(s) in the GML data more easily. Specifically, different normally distributed damage mechanisms will appear as straight line(s).

In Figure 4, both incubation and propagation rates are assumed to be constant for a given set of exposure conditions, with the Weibull modulus and characteristic lifetime generating a family of times at which propagation can be said to begin, with increasing probability of propagation having started (which may be considered to be a larger fraction of the exposed surface) as exposure time increases.

Data for 2 different deposit fluxes (1.5 and 5 $\mu g.cm^{-2}.h^{-1}$) and 'no deposit' are shown in Figure 4. All three conditions appear to have comparable incubation rates as shown in Figure 5, i.e. k_{inc} appears similar for Equation 1(a) and Equation 1(b). This indicates that there is

only a weak correlation between the deposit flux and incubation rate and is especially apparent in the case where no deposit is applied and hot corrosion incubation can be expected to be maintained indefinitely. Equation 3 gives the link between k_{inc} and deposit flux.

However both the rate of propagation and the Weibull parameters differ with changing deposit flux. Higher fluxes result in shorter characteristic incubation lifetimes and higher Weibull moduli (corresponding to tighter distributions of incubation lifetimes). This mirrors the fact that samples exposed to higher deposit fluxes move into propagation more rapidly. Additionally, the propagation rate appears to increase with increasing flux according to Equation 4.

$$k_{inc} = 0.0024f + 0.0157 \quad (3)$$

$$k_{prop} = 0.014f + 0.1525 \quad (4)$$

Where f is the flux (in $\mu g.cm^{-2}.h^{-1}$) and the rates are in $\mu m.h^{-1}$.

When no deposit is applied, MarM 509 is not observed to move out of incubation in the 500 hours of testing exposure. As such, no Weibull parameters or propagation rate can be determined for this set of conditions and it is predicted to remain in incubation indefinitely. As hot corrosion requires the presence of various deposits to initiate the fluxing mechanism which results in GML propagation, this is the expected result.

By looking at the range of GML values that the model predicts for the three different fluxes after 500 hours, comparisons can be made to the experimental data. Figure 6 shows similar

ranges of GML value can be produced, although there is some under prediction for regions of the sample which move into propagation earliest. Additionally, while the model shows a more pronounced distinction between regions of the sample in incubation and propagation, similar area fractions may be observed.

3.3 Modelling MarM 509 GML for Different Simulated Combusted Environments

Of the two other simulated combusted gas environments in the H2-IGCC project, the simulated combusted natural gas samples (6% CO_2-8% O_2-10% H_2O with 3.6 vpm SO_2 in N_2; Table 2) did not move out of incubation within the 500 hours of testing (Figure 7), and so the model has not been extended to this dataset. This behaviour can be confirmed from the SEM micrographs of the exposed samples (Figure 2(b)). The long incubation lifetime is an effect of the low SO_X and H_2O contents for this gas.

Figure 8 shows the GML cumulative probability distributions for MarM 509 following 500 hours exposure to deposit 3 at 700 °C in simulated combusted H_2-rich syngas (1% CO_2-8% O_2-20% H_2O with 3.6 vpm SO_2 in N_2; Table 2). While the overall extent of hot corrosion GML is lower than for the simulated combusted partially cleaned syngas, both deposits 2 and 3 (fluxes of 1.5 and 5 $\mu g.cm^{-2}.h^{-1}$) show propagation after 500 hours. Figure 2(c) also shows the formation of sulphur and oxide containing scales on the exposed samples surface.

The model outputs are shown in Figure 9. Compared to the simulated combusted partially cleaned syngas environment, the propagation rate is lower, and the range of incubation lifetimes larger.

3.4 Modelling MarM 509 GML for Different Temperatures

The model can be extended to datasets collected at 900 °C (type I hot corrosion). SEM micrographs in Figure 10 show that, after 500 hours exposure to the simulated combusted partially cleaned syngas environment the MarM 509 is undergoing hot corrosion attack. For the modelling work, samples exposed to deposit 2 (1.5 $\mu g.cm^{-2}.h^{-1}$ of 4/1 sodium/potassium sulphate) were compared for the two different temperatures (700 °C and 900 °C) as deposit 3, the most aggressive deposit at 700 °C, was not used at 900 °C. Instead, a 1.5 $\mu g.cm^{-2}.h^{-1}$ flux of pure sodium sulphate (deposit 4) had been used as the third deport flux/composition at 900 °C (as justified within [12]).

Figure 11 shows a comparison of the models for MarM 509 at 700 and 900 °C. While both temperatures appear to result in similar incubation rates and spreads in incubation lifetimes, the 700 °C model has a higher propagation rate under these conditions, leading to more extensive GML values.

3.5 Modelling Rene 80 GML

Figure 12 shows hot corrosion damage model outputs for Rene 80 samples exposed at 700 °C to simulated, combusted partially cleaned syngas with different fluxes of 4/1 sodium/potassium sulphate. Rene 80 produces a larger spread of incubation damage rates than MarM 509 (Figure 4). It can be seen that the incubation rate for Rene 80 exposed with deposit 2 (1.5 $\mu g.cm^{-2}.h^{-1}$) results in a steeper gradient (faster k_{inc}) than for no deposit or deposit 3 (5 $\mu g.cm^{-2}.h^{-1}$). By contrast MarM 509 shows relatively similar incubation rates (k_{inc} values) for all 3 deposit conditions. The variation for MarM 509 may be due to the experimental measurement accuracy of very small changes in GML while an area of a sample is under hot corrosion incubation.

The spread in incubation lifetimes according to the Weibull statistics is more confined for Rene 80 than MarM 509. This can be seen by the reduced spread in the lines that indicate the different probabilities.

3.6 GML Predictions for MarM 509

Following the production of the GML models, predictions about the extent and degree of hot corrosion damage can be made for samples exposed under conditions relevant to H_2-IGCC plant. As there are several alternative failure criteria for components, different methods of using the models can be considered to link exposure conditions to materials performance. For example:

- Figure 6 illustrates that the spread in expected GML values (after exposure to specific hot corrosion conditions for a defined time period) can be predicted.

- Figure 13 illustrates a plot of how long it will take for a specific degree of GML to have occurred with different probabilities.

- The models may also be used to predict the time taken to reach a certain amount of metal loss for different fractions of the sample (or cumulative probabilities), as shown in Figure 14.

It should be noted that in order to illustrate these potential application routes, the models have been used to times significantly beyond the 500 hours exposure data on which they were based and, as such, these long-time extrapolations should be treated with caution. On-going

and future work will investigate the validity of such extrapolations and also the interpolation of the existing model parameters to as yet untested exposure conditions.

4. Conclusions

This paper focuses on the results obtained from the exposures of MarM 509 and Rene 80 in three novel environments (simulating combusted partially cleaned syngas, natural gas, and H_2-rich syngas) using a range of deposition fluxes at 700 and 900 °C for periods of up to 500 hours. The models generated have been based on the concept of hot corrosion reactions following a two stage process (incubation followed by propagation) in which the duration of the incubation stage can be described using Weibull statistics.

The data generated have enabled the constants in the proposed hot corrosion framework model to be evaluated for both MarM 509 and Rene 80 for a range of exposure conditions. This has provided a quantitative and statistically based link between metal damage levels, deposition fluxes, gas compositions and metal temperatures for both alloys. The resulting models have been used to illustrate different approaches to predicting hot corrosion damage in the IGTs needed in advanced IGCC power plants. Further work is required to validate and extend the scope of such hot corrosion models, which can be considered for application to any other system undergoing incubation-propagation type damage mechanisms, assuming that suitable data has been collected.

Acknowledgements

The authors would like to acknowledge the support of the European Union's Framework 7 H2-IGCC project (grant number FP7-239349).

5. References

[1] P. Dechamps *Materials for Power Engineering*, Forschungszentrum Jülich **2006**

[2] European Commission, Communication from the Commission to the European Parliament, the Council, the European Economic and Social Committee and the Committee of the Regions: *A Roadmap for Moving to a Competitive Low Carbon Economy in 2050*, Reference: COM/2011/0112 final. **2011**

[3] C. C. Cormos, *Int. J. Hydrogen Energ.* **2009**, *34*, pp 6065.

[4] O. Maurstad, *An overview of coal based integrated gasification combined cycle (IGCC) technology*, Technical publication, MIT LFEE 2005-002 WP 2005

[5] N. J. Simms, J. Sumner, T. Hussain, J. E. Oakey, *Mater. Sci. Tech.* **2013**, *29*, pp 804.

[6] C. T. Campbell, *Surf. Sci.* **1987**, *183*, pp 100.

[7] D. S. Newsome DS, *Catal. Rev.* **1980**, *21*, pp 275.

[8] W. Nowak, *PhD. Thesis*, RWTH Aachen, Germany, Lehrstuhl für Werkstoffe der Energietechnik (FZ Jülich) 2014.

[9] M. C. Maris-Sida, G. H. Meier, F. S. Pettit, *Metal. Mater. Trans. A.* **2003**, *34(11)*, pp 2609.

[10] C. Duret-Thual, R. Morbioli, P. Steinmetz, *A Guide to the Control of High Temperature Corrosion and Protection of Gas Turbine Materials*, Commission of the European Communities, Belgium **1986**

[11] K. P. Lillerud, P. Kofstad, *Oxid. Met.* **1984**, *21*, pp 233

[12] J. Sumner, A. Potter, N. J. Simms, J. E. Oakey, *Mater. High Temp.* **2015**, *32*, pp177

[13] J. Sumner, A. Potter, N. J. Simms, J. E. Oakey, presented at *7th International Gas Turbine Conference*, Brussels, Belgium, 14-15 October, **2014**, pp.1-10.

[14] BSI Standards, *Corrosion of Metals and Alloys – Test Method for High Temperature Corrosion Testing of Metallic Materials by Application of a Deposit of Salt, Ash, or Other Substance*, BS ISO 17224:**2015.**

[15] BSI Standards, *Corrosion of Metals and Alloys – Test Method for High Temperature Corrosion Testing of Metallic Materials by Immersing in Molten Salt or Other Liquids under Static Conditions,* BS ISO 17245:**2015.**

[16] BSI Standards, *Corrosion of Metals and Alloys – Test Method for High Temperature Corrosion Testing of Metallic Materials by Embedding in Salt, Ash, or Other Solids*, BS ISO 17248:**2015.**

[17] BSI Standards, *Corrosion of Metals and Alloys – Test Methods for Isothermal-Exposure Oxidation Testing under High-Temperature Corrosion Conditions for Metallic Materials*, BS ISO 21608:**2012.**

[18] N. J. Simms, J. R. Nicholls, J. E. Oakey, *Mater. Sci. Forum*, **2001**, *369*, pp.833.

[19] M. Kowaka, *Introduction to Life Prediction of Industrial Plant Materials: Application of the Extreme Value Statistical Method for Corrosion Analysis*, Allerton Press, New York **1994.**

[20] D. J. Sweeney, T. A. Williams, D. R. Anderson, *Fundamentals of Business Statistics, 5th Edition,* South-Western Cengege Learning, Australia, **2006.**

[21] D. J. Hand, *Statistics: A Very Short Introduction*, Oxford University Press, UK, **2008.**

[22] BSI Standards, *Corrosion of Metals and Alloys – Guidelines for Applying Statistics to Analysis of Corrosion Data*, BS ISO 14802:**2012.**

[23] J. Sumner, A. Encinas-Oropesa, N. J. Simms, J. R. Nicholls, *Mater. Corros.* **2014**, *65*, pp.188.

[24] J. R. Nicholls, P. Hancock, *High Temperature Corrosion* (ed. R. A. Rapp), NACE, pp.198-210, **1983.**

[25] N. J. Simms, P. J. Smith, A. Encinas-Oropesa, S. Ryder, J. R. Nicholls, J. E. Oakey, *Lifetime Modelling of High Temperature Corrosion Processes* (ed. M. Schütze, W. J. Quadakkers, J. R. Nicholls), Maney, pp.246-260, **2001.**

[26] BSI Standards, *Corrosion of Metals and Alloys – Methods for Metallographiuc Examination of Samples after Exposure to High-Temperature Corrosive Environments*, BS ISO 26146:**2012**

[27] BSI Standards, *Corrosion of Metals and Alloys – Test Method for Thermal-Cycling Exposure Testing under High-Temperature Corrosion Conditions for Metallic Materials*, BS ISO 13573:**2012.**

[28] S. Osgerby, T. Fry, *Mat. Res.* **2004**, *7(1)*, pp. 141.

[29] X. Montero, M. C. Galetz, *Oxid. Met.* **2015**, *83* pp. 485.

Received: ((will be filled in by the editorial staff))

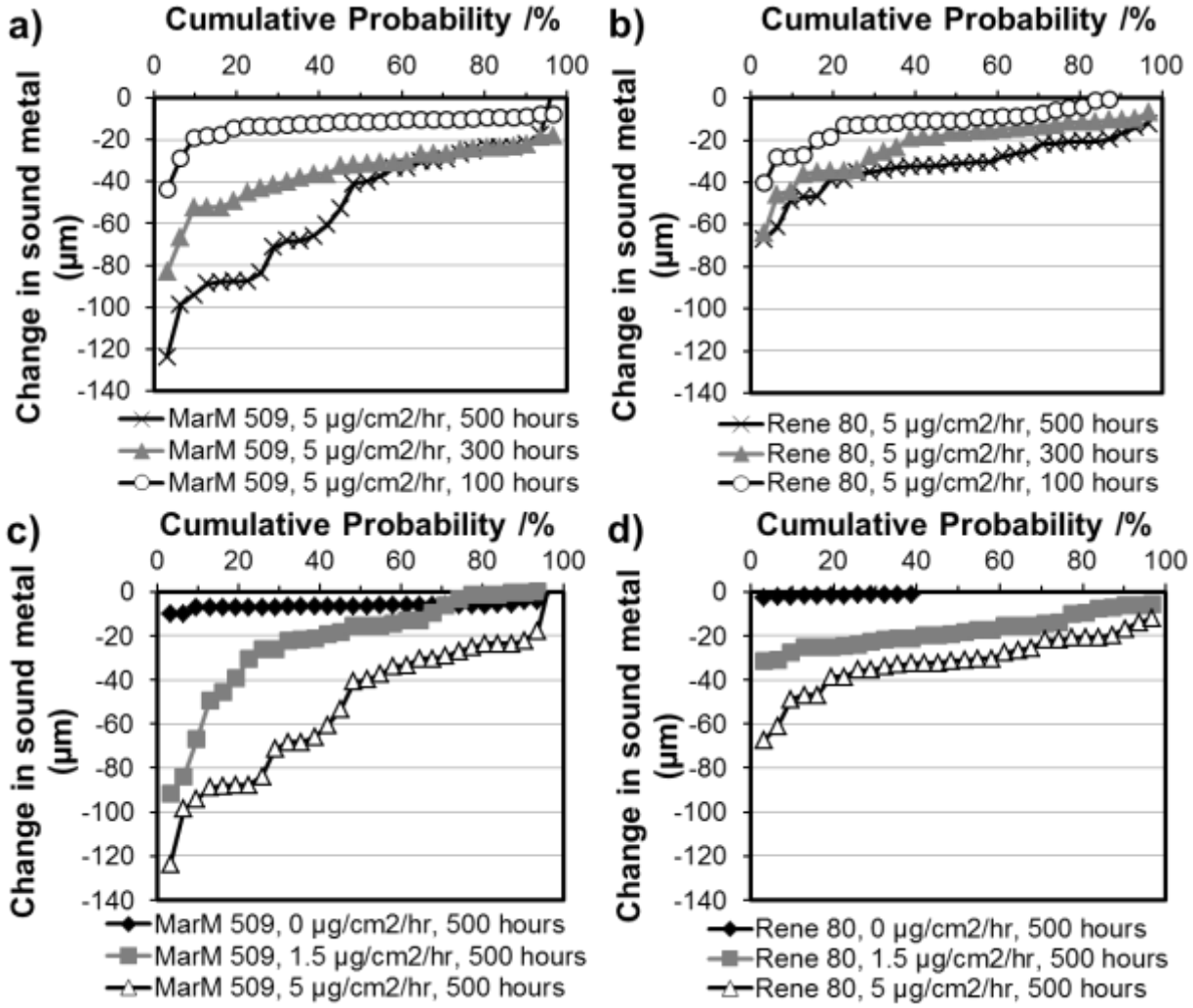

Figure 1. Example cumulative probability plots showing GML for (a,c) MarM 509 and (b,d) Rene 80. (a,b) show effect of different exposure times for deposit 3, while (c,d) show effect of changing deposit flux after 500 hours. Testing carried out in simulated combusted partially cleaned syngas at 700 °C.

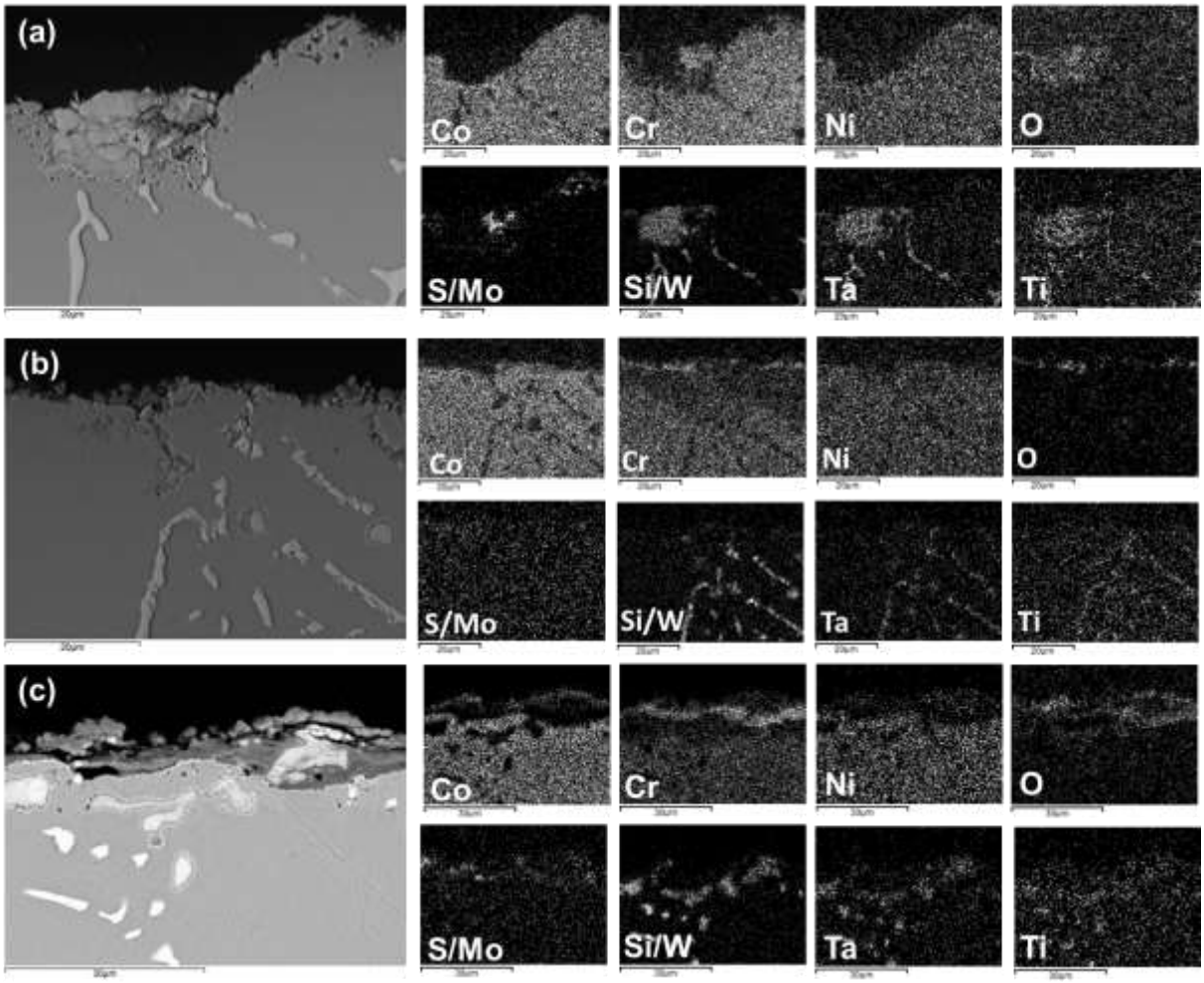

Figure 2. SEM back scattered electron micrographs and corresponding EDX maps for MarM 509 in (a) simulated, combusted partially cleaned syngas; (b) simulated, combusted natural gas syngas; and (c) simulated, combusted H_2-rich syngas. All micrographs taken after 500 hours exposure with deposit 3 at 700 °C.

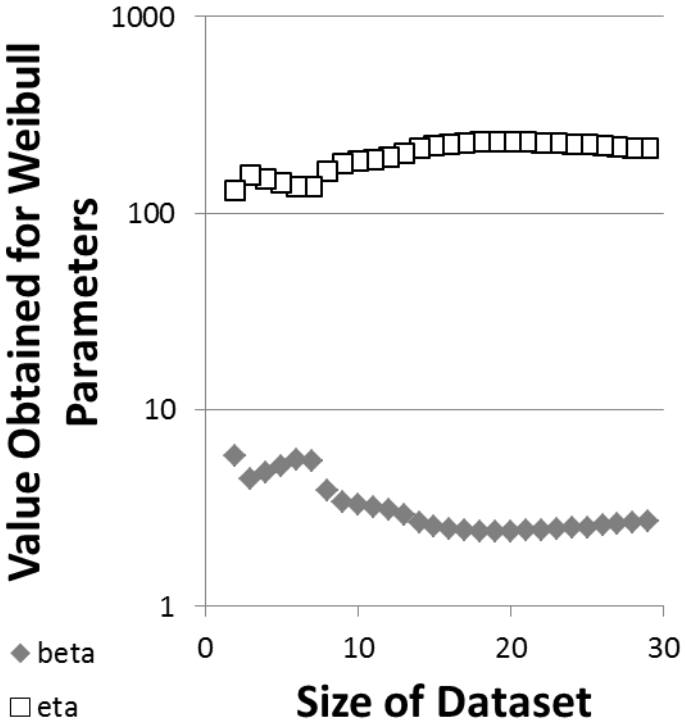

Figure 3. Sensitivity of Weibull parameters β and η to the numbers of input data.

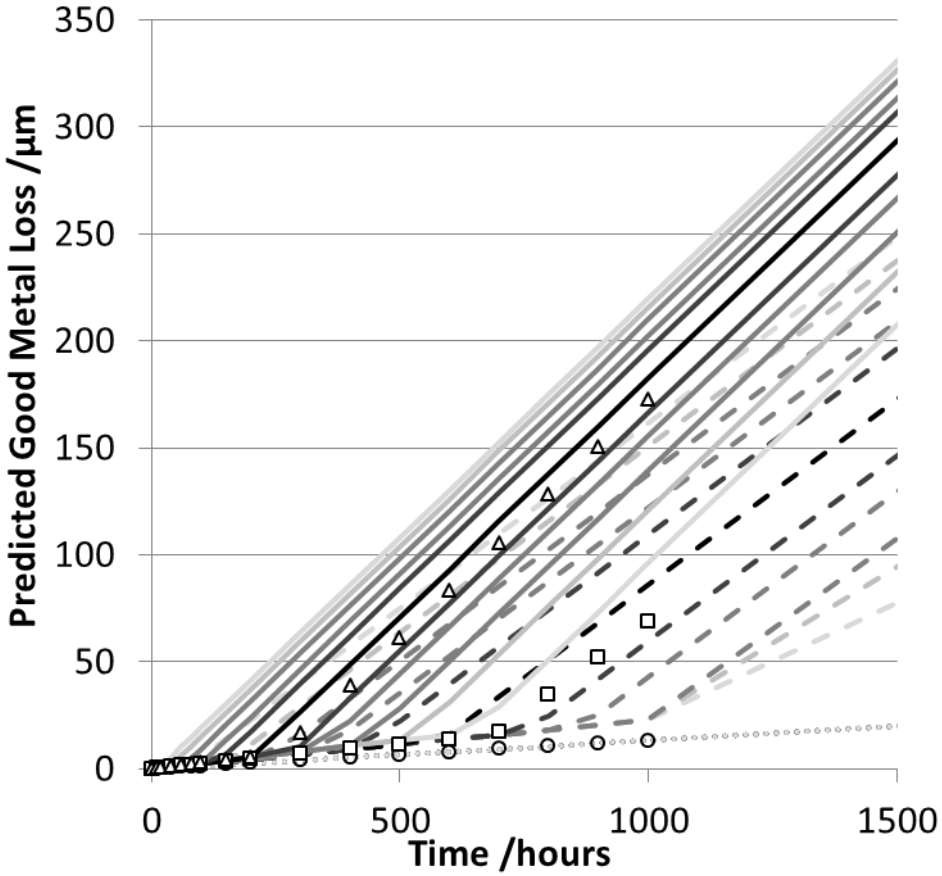

Figure 4. Examples of hot corrosion damage model outputs. Data for MarM 509 samples exposed at 700 °C to simulated, combusted partially cleaned syngas with different fluxes of 4/1 sodium/potassium sulphate. Solid lines are for deposit 3. Dashed lines are for deposit 2. Dotted lines are for no deposit. Characteristic lifetimes are given by triangles (5 $\mu g.cm^{-2}.h^{-1}$), squares (1.5 $\mu g.cm^{-2}.h^{-1}$) and circles (no deposit). Probabilities plotted are: 0.99 (lightest shade), 0.96, 0.9, 0.8, 0.7, 0.5 (darkest shade), 0.3, 0.2, 0.1, 0.04, 0.01 (lightest shade).

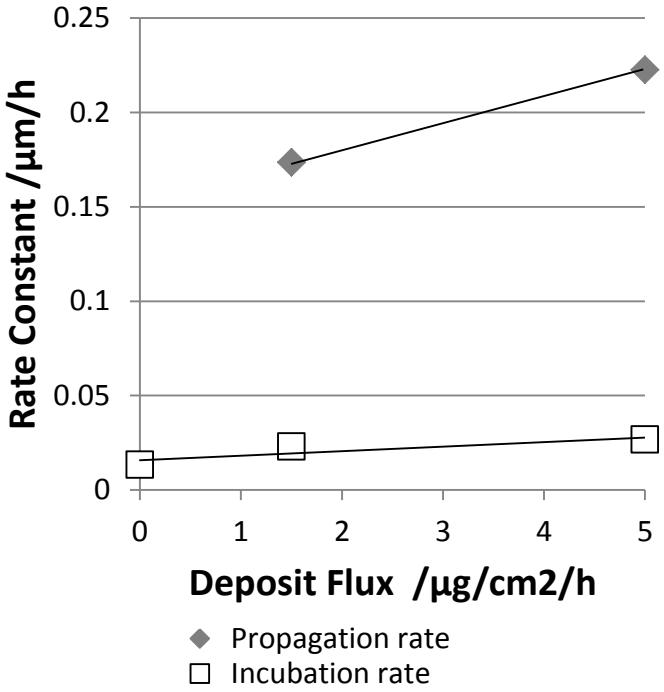

Figure 5. Variation in incubation and propagation rates with deposit flux for MarM 509 in simulated combusted partially cleaned syngas at 700 °C.

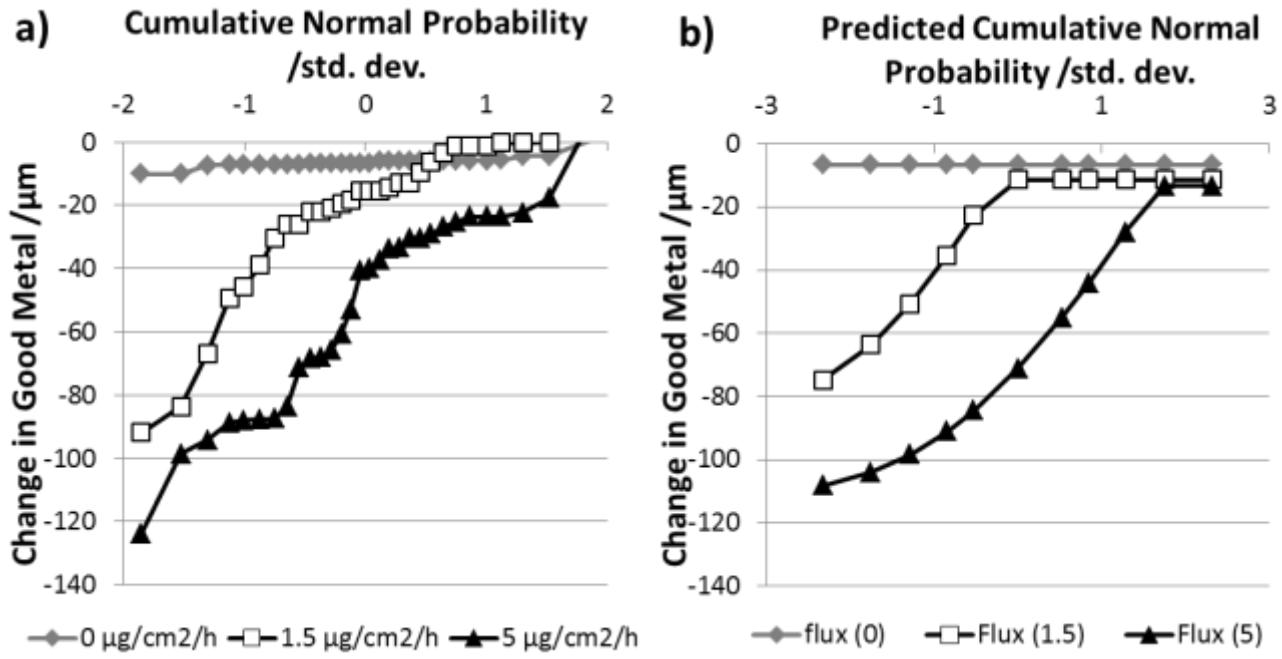

Figure 6. Comparison of (a) dimensional metrology data taken after 500 hours and (b) the predicted data from the model for deposits 1 - 3. Data for MarM 509 in simulated combusted partially cleaned syngas at 700 °C.

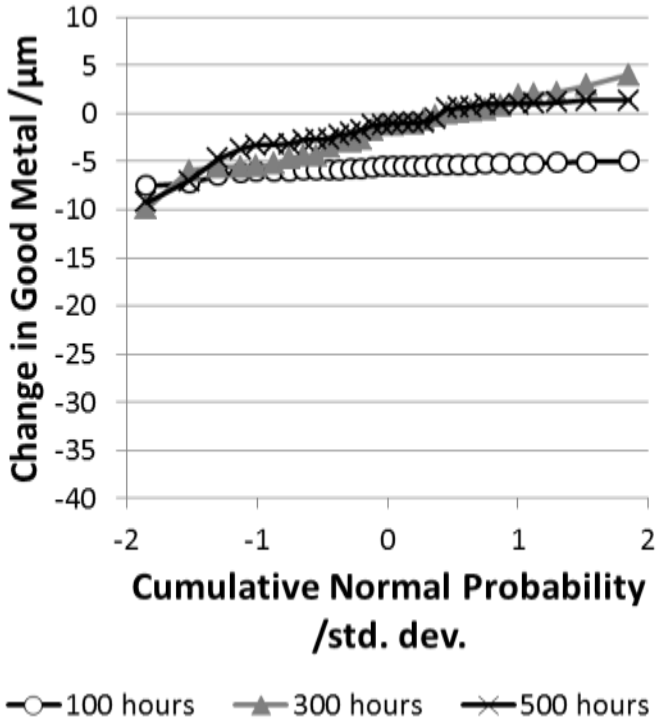

Figure 7. Cumulative probability plots showing MarM 509 GML variation with time following exposure to deposit 3 at 700 °C in simulated combusted natural gas. (Note that this measurement technique has an error of ±5 µm.)

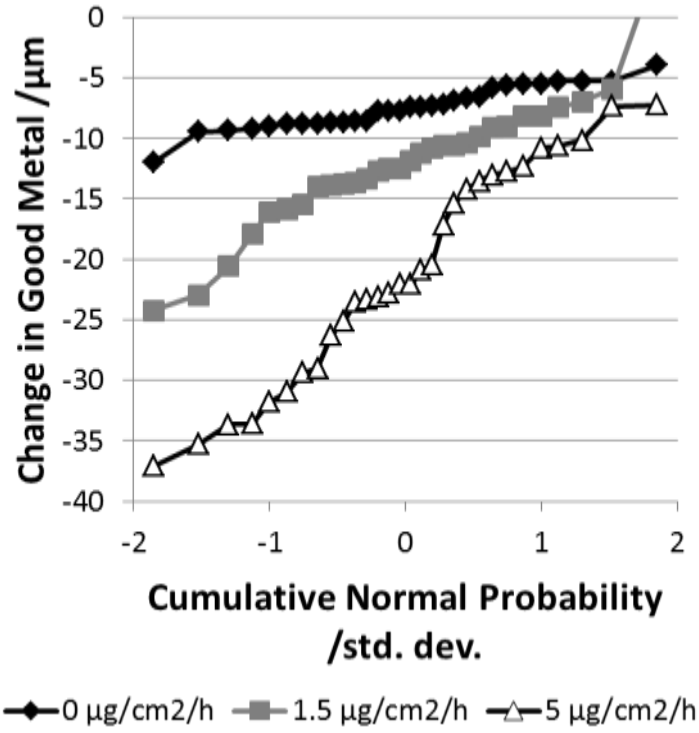

Figure 8. Cumulative probability plots showing MarM 509 GML variation with deposit flux following 500 hours exposure to deposit 3 at 700 °C in simulated combusted H_2-rich syngas.

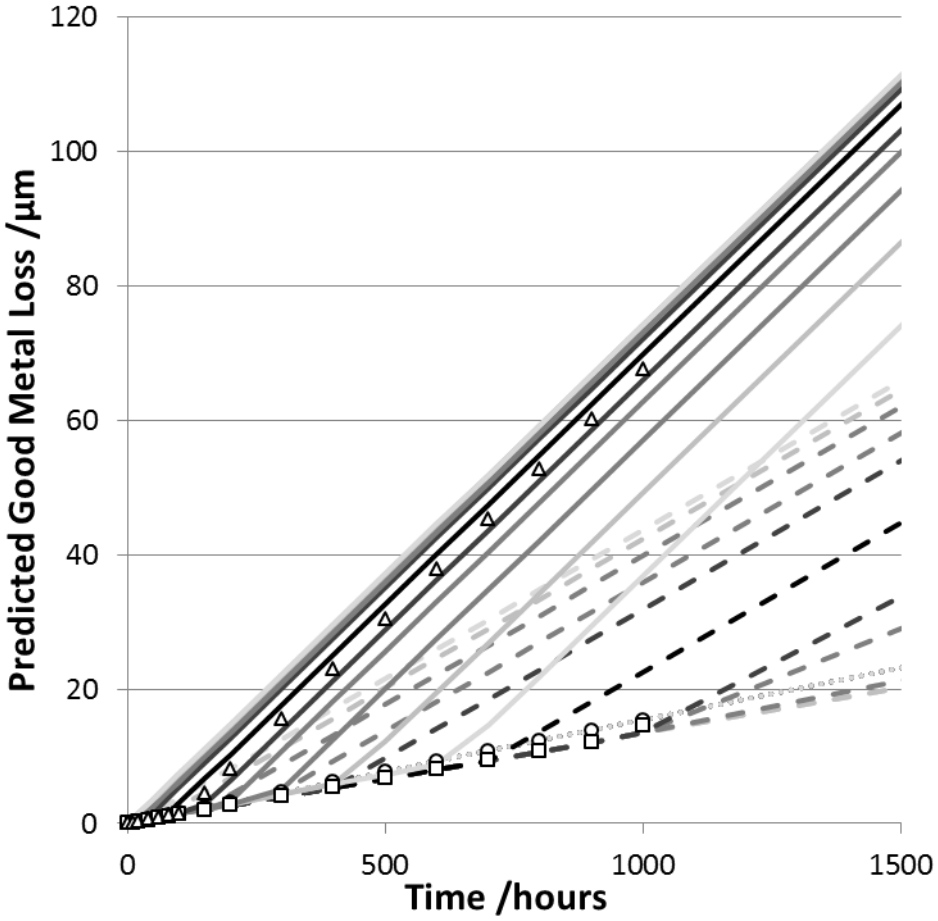

Figure 9. Hot corrosion damage model outputs for MarM 509 exposed at 700 °C to simulated, combusted H_2-rich syngas with different fluxes of 4/1 sodium/potassium sulphate. Solid lines are for deposit 3. Dashed lines are for deposit 2. Dotted lines are for no deposit. Characteristic lifetimes are given by triangles (5 µg.cm^{-2}.h^{-1}), squares (1.5 µg.cm^{-2}.h^{-1}) and circles (no deposit). Probabilities plotted are: 0.99 (lightest shade), 0.96, 0.9, 0.8, 0.7, 0.5 (darkest shade), 0.3, 0.2, 0.1, 0.04, 0.01 (lightest shade).

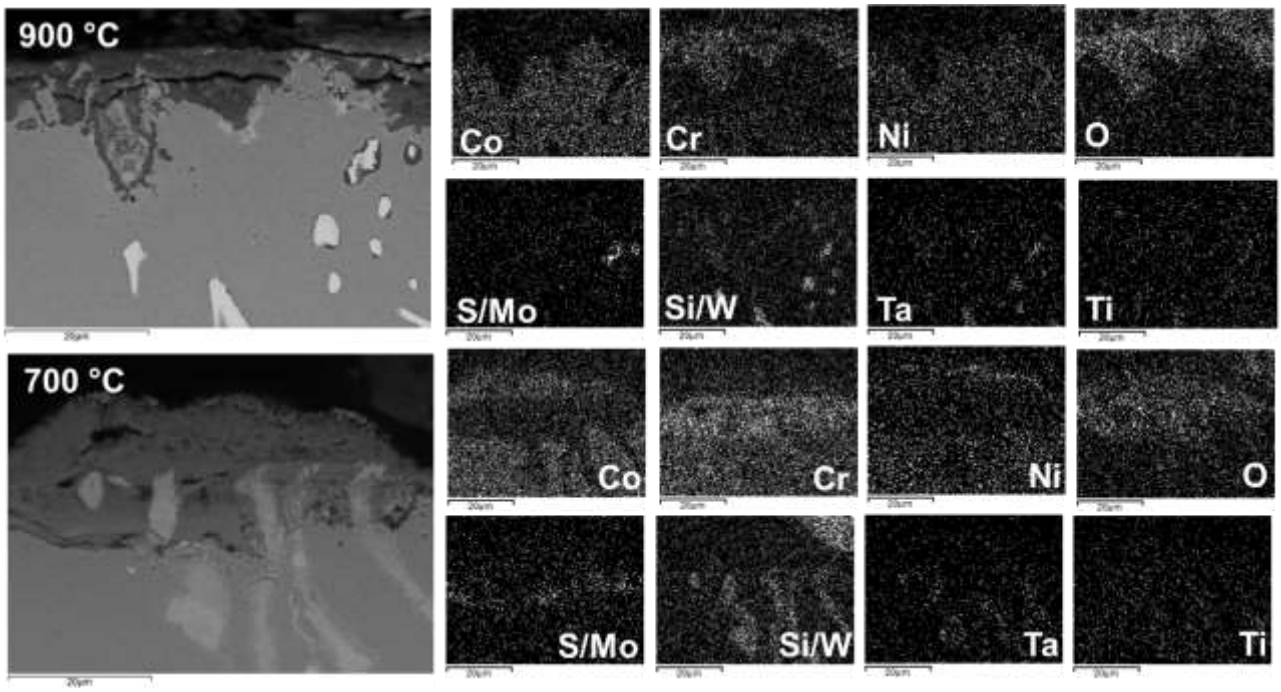

Figure 10. SEM back scattered electron micrographs and corresponding EDX maps for MarM 509 in simulated, combusted partially cleaned syngas after 500 hours exposure with deposit 2 at (top) 900 °C and (bottom) 700 °C.

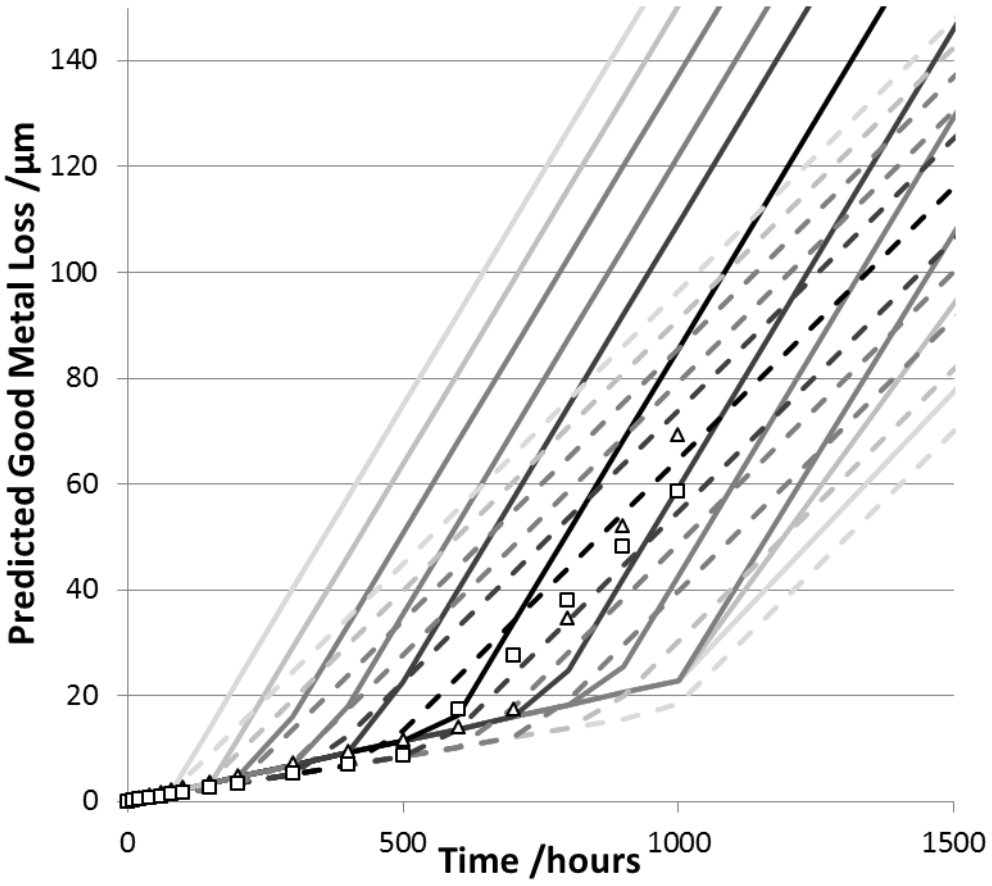

Figure 11. Hot corrosion damage model outputs for MarM 509 exposed to simulated, combusted partially cleaned syngas a 1.5 µg.cm^{-2}.h^{-1} flux of 4/1 sodium/potassium sulphate. Solid lines are for 700 °C. Dashed lines are for 900 °C. Characteristic lifetimes are given by triangles (700 °C), and squares (900 °C). Probabilities plotted are: 0.99 (lightest shade), 0.96, 0.9, 0.8, 0.7, 0.5 (darkest shade), 0.3, 0.2, 0.1, 0.04, 0.01 (lightest shade).

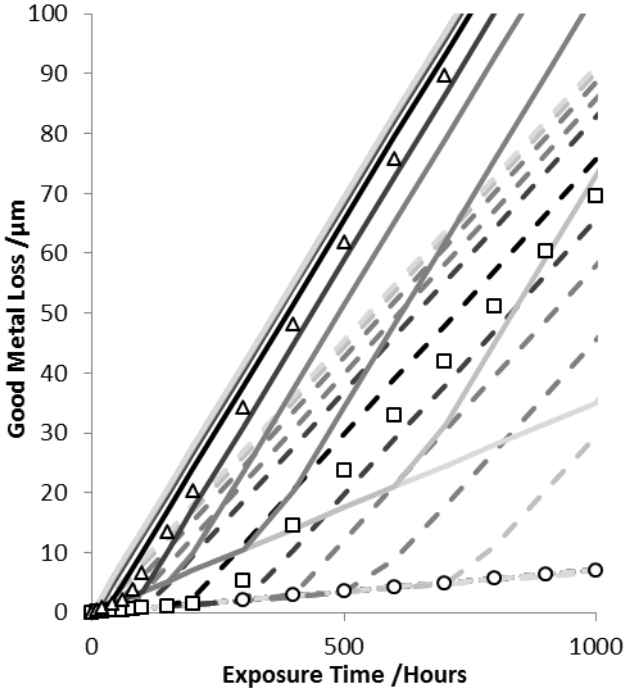

Figure 12. Hot corrosion damage model outputs. Data for Rene 80 samples exposed at 700 °C to simulated, combusted partially cleaned syngas with different fluxes of 4/1 sodium/potassium sulphate. Solid lines are for deposit 3. Dashed lines are for deposit 2. Dotted lines are for no deposit. Characteristic lifetimes are given by triangles (5 $\mu g.cm^{-2}.h^{-1}$), squares (1.5 $\mu g.cm^{-2}.h^{-1}$) and circles (no deposit). Probabilities plotted are: 0.99 (lightest shade), 0.96, 0.9, 0.8, 0.7, 0.5 (darkest shade), 0.3, 0.2, 0.1, 0.04, 0.01 (lightest shade).

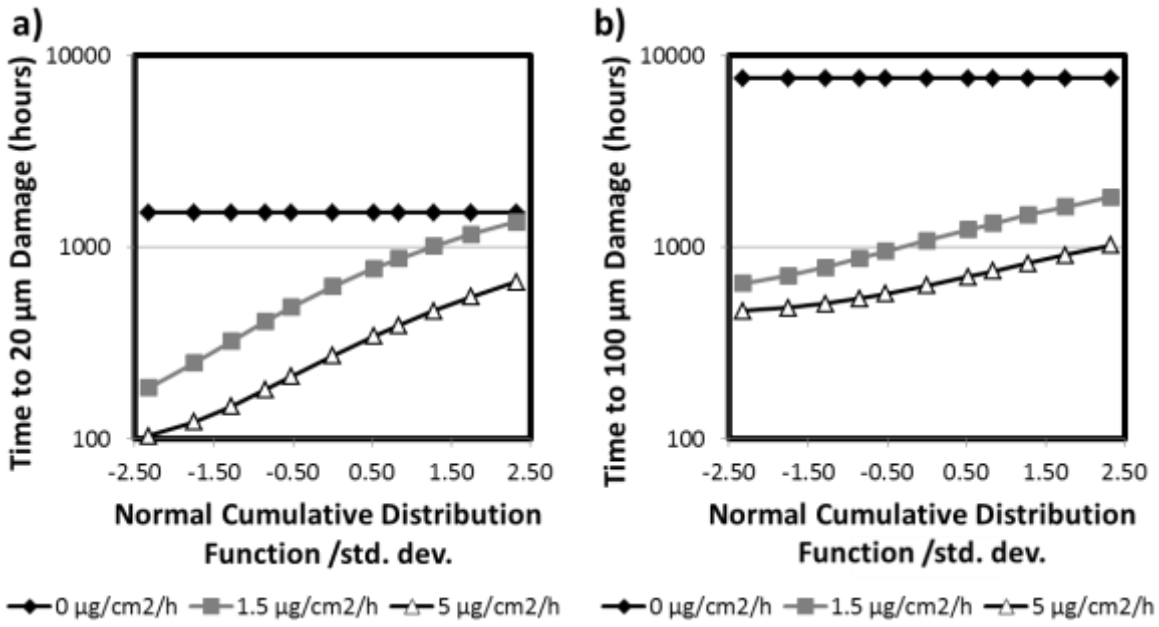

Figure 13. Predictions for the time taken for (a) 20 µm and (b) 100 µm of GML for MarM 509 exposed at 700 °C to the simulated, combusted partially cleaned syngas with different fluxes of 4/1 sodium/potassium sulphate.

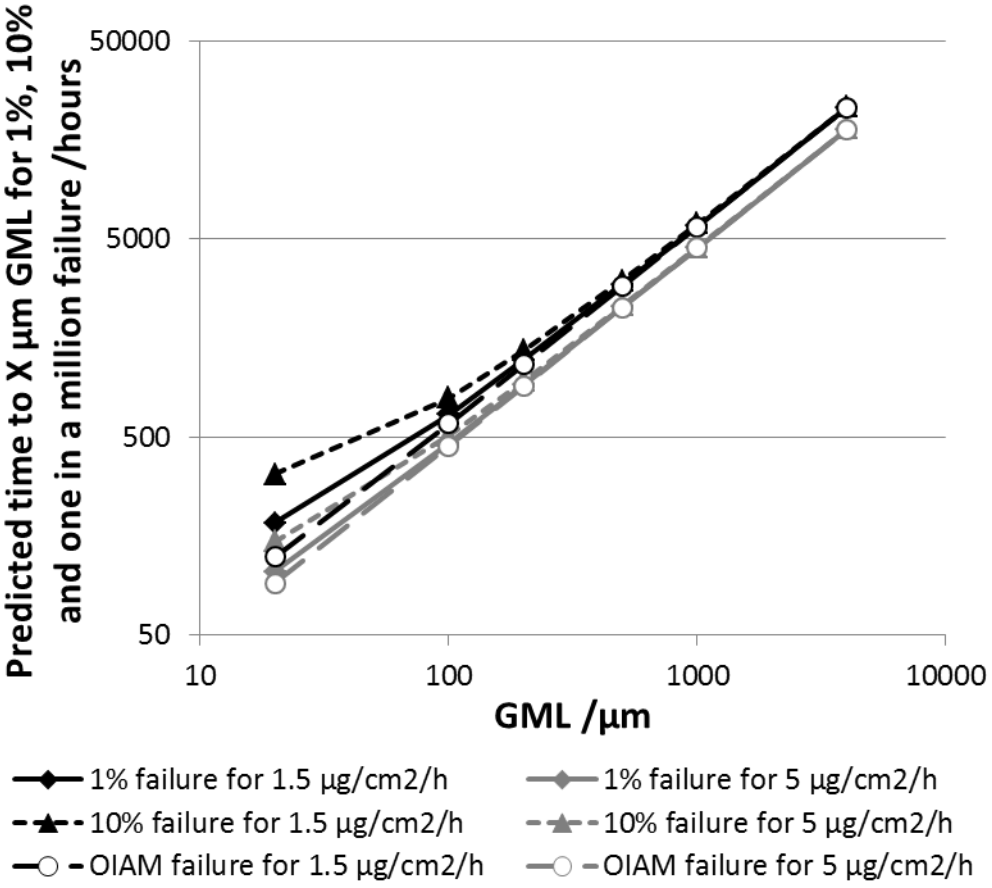

Figure 14. Predictions for the time taken to reach a certain amount of metal loss. Different lines correspond to different fractions of the sample achieving the GML value. Plots made for MarM 509 exposed to deposits 2 and 3at 700 °C in the simulated, combusted partially cleaned syngas. (OIAM: one in a million.)

Table 1. Composition of the two substrate alloys (wt.%; b: balance)

Alloy	Ni	Cr	Co	Ti	W	Al	Ta	Mo	C	B	Zr
Rene 80	b	14	9.5	5	4	3	…	4	0.16	0.015	0.03
MarM 509	10	23.5	b	0.2	7	…	3.5	…	0.6	…	0.5

Table 2. Compositions of the 3 gases used in the furnace tests. N_2 balance. (vpm: volumes per million)

Combusted gas simulated	**CO_2**	**O_2**	**SO_2**	**H_2O**
H_2-rich syngas	1%	8%	3.6 vpm	20%
Natural gas	6%	8%	3.6 vpm	10%
Partially cleaned syngas	10%	8%	86.4 vpm	5%

Table 3. The 4 combinations of deposit composition/flux covered in this paper. Note that not all combinations were used at all temperatures.

#	Deposit Flux /µg.cm^{-2}.h^{-1}	Deposit Composition	Used at Temperature /°C
1	0	No Deposit	700, 900
2	1.5	80:20 Na_2SO_4:K_2SO_4	700, 900
3	5	80:20 Na_2SO_4:K_2SO_4	700
4	1.5	100% Na_2SO_4	900

Graphical Abstract

A framework model to predict hot corrosion damage has been produced based on a 2-stage corrosion process (initiation & propagation). Weibull statistics are used to assess the spread in incubation lifetime & final damage distribution. Data populating the model comes from laboratory tests simulating potential integrated gasification combined cycles firing industrial gas turbines on H_2-rich syngas.

The table of contents (ToC) entry should be up to 400 characters long. The entry should be written in the present tense and impersonal style. The text should be different from the abstract text.

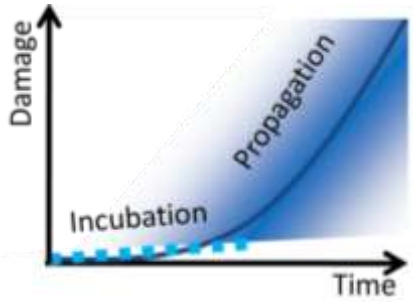

ToC figure ((Please choose one from your article or one specifically designed.
Size: about 55 mm broad. No caption.))